International Communications in Heat and Mass Transfer 155 (2024) 107553

Contents lists available at ScienceDirect

International Communications in Heat and Mass Transfer

journal homepage: www.elsevier.com/locate/ichmt

Geometrical investigation of forced convective flows over staggered arrangement of cylinders employing constructal design

Ana Paula Del Aghenese [a], Claudia Naldi [b,*], Luiz Alberto Oliveira Rocha [a,c], Liércio André Isoldi [a,c], João Francisco Prolo Filho [c], Cesare Biserni [b], Elizaldo Domingues dos Santos [a,c]

[a] Graduate Program of Computational Modeling, School of Engineering, Federal University of Rio Grande (FURG), Italia Avenue, km 8, Rio Grande, RS, Brazil
[b] Department of Industrial Engineering (DIN), Alma Mater Studiorum - University of Bologna, Bologna, Italy
[c] Graduate Program of Ocean Engineering, School of Engineering, Federal University of Rio Grande (FURG), Italia Avenue, km 8, Rio Grande, RS, Brazil

ARTICLE INFO

Keywords:
Constructal design
Forced convection
Arrangement of cylinders
Staggered configuration
Longitudinal pitches

ABSTRACT

The current numerical work conducted a geometrical investigation of forced convective flows over a staggered arrangement of four cylinders applying constructal design. The main objectives are to determine designs maximizing the Nusselt number (Nu_D) and minimizing the drag coefficient (C_D) of the cylinders at three distinct Reynolds numbers ($Re_D = 10$, 40, and 150) considering $Pr = 0.71$. The problem involves two constraints: cross-sectional area of the cylinders and the occupation area of the arrangement, and three degrees of freedom: S_T/D, S_{L1}/D and S_{L2}/D. These represent the ratios between the transversal pitch, the longitudinal pitch between the frontal and intermediate cylinders, and the longitudinal pitch between the intermediate and posterior cylinders over the diameter. The introduction of two longitudinal pitches enabled an exploration of the generation of asymmetrical patterns in the flow direction. Results indicated a strong dependency of the arrangement design on the Reynolds number. Moreover, asymmetrical configurations generally benefited both performance indicators for the present conditions. The most favorable arrangements for the fluid dynamics were achieved with the lowest S_T/D, more concentrated longitudinal pitches for $Re_D = 10$, and asymmetrical pitches for $Re_D = 40$ and 150. Concerning the thermal purpose, the highest magnitude of S_T/D and asymmetrical longitudinal pitches led to the highest Nu_D. For $Re_D = 10$, the intermediate cylinders are near the upstream one; for $Re_D = 40$ the length of the arrangement increases with the intermediate cylinders near the downstream one, and for $Re_D = 150$, the arrangement occupied all the length of occupation area with slight asymmetry.

1. Introduction

Convection heat transfer flows over arrangement of tubes or cylinders has attracted particular interest due to its accurate representation of various industrial and commercial equipment, including heat exchangers, evaporators, condensers, and other engineering applications as electronic packaging, gas pipelines, and air-conditioning units [1–3]. Moreover, the complex structures generated in the flow over a single cylinder, such as boundary layer detachment, vortex shedding and formation of vortex street, along with the interaction of multiple structures in an arrangement of cylinders, pose a challenging issue for the accurate prediction of their design [4–6].

Several studies have been reported in the literature aiming to define strategies to enhance the heat transfer between one cylinder and the surrounding flow. These strategies include the consideration of protrusions [7], the incorporation of multiple fins in the cylinder periphery [8], or the use of flexible fins [9] to passively control the flow. These studies also focus on the understanding the flow behavior once the use of protrusions or fins dramatically alters the flow regime, leading to changes in the vortex shedding that can result in synchronization with the natural frequency of the material (lock-on phenomenon) [8]. In addition to circular cylinders and those with protrusions or fins, other geometric configurations, such as square/rectangular shapes, have also been extensively studied [10]. Alternative configurations as semi-circular cylinder [11], cam-shaped cylinder [12], and elliptical and wave elliptical cylinders [13,14] have also been reported. A comprehensive review on the influence of different geometrical configurations for a single cylinder over the behavior of fluid flow is described in the

* Corresponding author.
E-mail address: claudia.naldi2@unibo.it (C. Naldi).

https://doi.org/10.1016/j.icheatmasstransfer.2024.107553
Received 5 March 2024; Received in revised form 29 April 2024; Accepted 5 May 2024
Available online 9 May 2024

work of Lekkala et al. [15]. Another strategy to augment the thermal exchange involves placing the cylinder in an enclosure, such as an expansion in a channel [16]. Recent advances have been done on the use of magnetohydrodynamics to control the fluid flow and augment the heat transfer rate between the cylinder and the fluid flow [17]. Studies on two tubes or bluff bodies under different configurations (in line, side-by-side or inclined) had also been reported in the literature. For instance, the work of Sumner [3] provides a detailed explanation about the behavior of the fluid flow over a pair of cylinders under several conditions. In general, the literature has demonstrated that the studies of convective flows over single or pair of cylinders remains a relevant issue.

Regarding advancements in the study of cylinder arrangements, investigations have been performed ranging from single rows to staggered and aligned configurations with three cylinders or more [18–22]. For instance, Ambesi and Kleijn [18] numerically studied forced convection laminar flows over a perpendicular single row of cylinders with equidistant and non-equidistant spacing. Authors explored the array's impact on the average Nusselt number for different Reynolds ($0.001 \leq Re_D \leq 600$) and Prandtl numbers ($0.7 \leq Pr \leq 10$). Authors noticed a decrease in the average Nusselt number of the array with the decrease of the open frontal area for low Reynolds numbers and equidistant cylinders. Furthermore, for the same frontal area, the non-equidistant array led to lower Nusselt numbers for intermediate Reynolds numbers, with no significant impact on heat transfer rates for low and high Reynolds numbers. Subsequently, Daróczy et al. [19] used computational intelligence to search for the best positions of seven-cylinders arrangement, aiming to maximize the heat transfer rate between the cylinders and the surrounding flow. Recently, Pravesh et al. [20] investigated mixed convective non-Newtonian flows over inline array of cylinders. The study considered different numbers of Reynolds ($1 \leq Re_D \leq 40$) and Prandtl ($1 \leq Pr \leq 50$), as well as varied power-law indexes ($0.4 \leq n \leq 1.8$). The configuration was assessed using a fluid volume fraction parameter, representing the fluid area over the total square area defined by $(L + D/2)^2$ where L is the distance among the cylinders and D the diameter. The investigation revealed an increase in the average Nusselt number with Reynolds, Prandtl and Richardson numbers for shear-thinning fluids (n tending to 0.4), while the opposite was observed for shear-thickening fluids (n tending to 1.8). Additionally, an increase in volume fraction resulted in a higher Nusselt number for mixed convective flows, contrary to observations in forced convective flows. Xue et al. [21] examined forced convective laminar flows over a bundle with 10 tubes using an equilateral triangle arrangement. The authors evaluated the influence of the Reynolds number, longitudinal and transversal pitches over the tube-averaged heat transfer and average friction coefficients. The study focused on varying one parameter while keeping the other two constant, i.e., it is not performed a combination of different pitches. Results indicated that the transversal pitch and Reynolds number had the most significant impact on the thermal and fluid dynamics performance. Finally, Islam et al. [22] made a numerical study investigating the influence of vibration of internal line of cylinders in an initially aligned arrangement with 3 × 3 cylinders. The study also explored the impact of transverse spacing ratio and the diameter on parameters such as mean pressure coefficient and Nusselt number. The best thermal performance was achieved when the varying cylinders have the lowest transverse spacing investigated, compared to arrangements with the same diameter.

As a finite size flow system, the design in convection heat transfer over arrangements of cylinders can be guided by the constructal law of design and evolution [23–25]. The constructal law is a physical principle that posits the design and rhythm in any finite-size flow system, whether animate or inanimate, evolves toward facilitating the internal currents that flow through the thermodynamical system. The constructal design, which is the method of application of the constructal law, has been utilized to demonstrate the designs in nature, society, and engineering applications [23–26]. In the external convection heat transfer flows, the method has been applied to investigate the geometry of fins that best remove heat from a basement [27], and to direct the configuration of aligned arrangement of cylinders subjected to natural convection [28], arrays of cylinders in rotation with different sizes under forced convection [29], triangular arrangement of cylinders, and bluff bodies under mixed and forced convection laminar flows [30,31]. Recent investigations have sought to understand the influence of the triangular arrangement of bluff bodies on drag coefficient and Nusselt number, considering turbulent mixed convection flows with $Re_D = 22{,}000$ and $Pr = 0.71$ [32]. Additionally, a construction function based on velocity and thermal fields has been employed to create an arrangement from an elementary configuration (with one tube) for forced convection laminar flows for three different Reynolds numbers ($Re_D = 10$, 50 and 100) and $Pr = 0.71$ [33]. Finally, Cunegatto et al. [34] associated the constructal design and response surface methodology to study the influence of arrangements of tubes with different sizes on heat transfer density for convection heat transfer flows and with pseudoplastic fluids.

The literature review evidenced several research works where the constructal design was successfully applied to direct the configuration of cylinders subjected to convective flows. Nevertheless, none of the previously mentioned investigations considered the influence of two different longitudinal pitches for the elementary lozenge configuration of the arrangement of cylinders over both the fluid dynamic and thermal performance. The present work aims to contribute in this regard by employing the constructal design method to investigate the influence of a staggered arrangement of four cylinders on the average drag coefficient (C_D) and average Nusselt number (Nu_D) in forced convective laminar flows. To explore the impact of variable longitudinal pitches in the arrangement design, the problem is defined with three degrees of freedom: S_T/D (the ratio between the transversal pitch of intermediate cylinders and the diameter of the cylinders), S_{L1}/D (the ratio between the longitudinal pitch of upstream and intermediate cylinders and the diameter of the cylinders), and S_{L2}/D (ratio between the longitudinal pitch of the intermediate cylinders and the downstream one and the diameter of the cylinders). Additionally, the effect of the Reynolds number on the best fluid dynamic and thermal configurations is investigated.

2. Mathematical and numerical modeling

2.1. Problem description and governing equations

The investigated problem involves an incompressible, laminar, forced convection flow of air ($Pr = 0.71$) over a staggered arrangement of cylinders in a two-dimensional domain, as illustrated in Fig. 1. The domain of Fig. 1 has the following constant dimensions: $D = 0.1$ m, $H = 15D = 1.5$ m, $L = 35D = 3.5$ m, $L_1 = 8D = 0.8$ m. The fluid flow is analyzed in the unsteady state, with C_D and Nu_D evaluations performed upon reaching a steady-state condition. The flow is induced by a prescribed velocity field at the inlet of the domain, and heat transfer occurs due to the temperature difference between the isothermal cylinders at a higher temperature ($T_w = 320$ K) and the cooler surrounding stream ($T_\infty = 300$ K). The specified boundary conditions include a constant velocity ($u = V_\infty$) with three potential values based on the Reynolds number, and a temperature ($T = T_\infty$) imposed on the left-lateral surface of the domain. The four cylinders exhibit constant velocity ($u = v = 0$ m/s) and temperature ($T = T_w$). Symmetry conditions are applied to the upper and lower surfaces of the domain, while a constant gauge pressure ($p_g = 0$ Pa) is maintained at the exit, represented by the right surface of the domain. It is worth mentioning that the domain's right surface is placed far enough from the four-cylinder array not to affect the results. Regarding initial conditions, the fluid is initially at rest ($u = v = 0$ m/s, $T = T_\infty$) at the starting time ($t = 0$ s).

The modeling of the forced convection problem is given by the following equations of conservation of mass, momentum in x and y directions, and conservation of energy [35]:

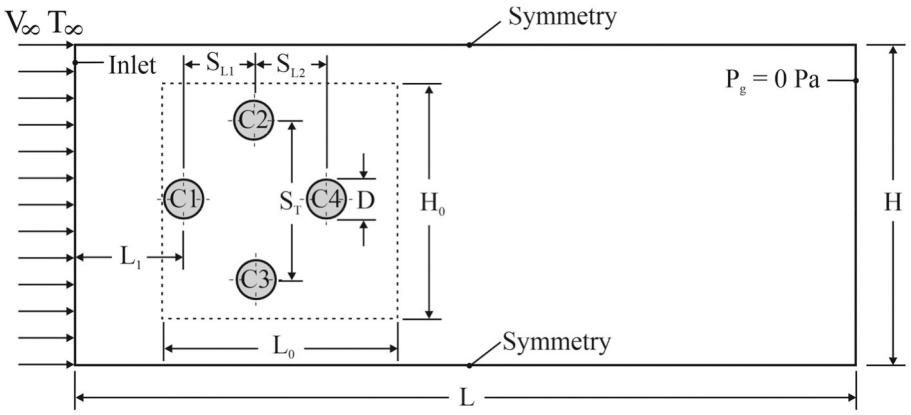

Fig. 1. Problem domain of the staggered arrangement of four cylinders subjected to forced convective flows.

$$\frac{\partial u}{\partial x}+\frac{\partial v}{\partial y}=0 \tag{1}$$

$$\frac{\partial u}{\partial t}+u\frac{\partial u}{\partial x}+v\frac{\partial u}{\partial y}=-\frac{1}{\rho}\frac{\partial p}{\partial x}+\upsilon\left(\frac{\partial^2 u}{\partial x^2}+\frac{\partial^2 u}{\partial y^2}\right) \tag{2}$$

$$\frac{\partial v}{\partial t}+u\frac{\partial v}{\partial x}+v\frac{\partial v}{\partial y}=-\frac{1}{\rho}\frac{\partial p}{\partial y}+\upsilon\left(\frac{\partial^2 v}{\partial x^2}+\frac{\partial^2 v}{\partial y^2}\right) \tag{3}$$

$$\frac{\partial T}{\partial t}+u\frac{\partial T}{\partial x}+v\frac{\partial T}{\partial y}=\alpha\left(\frac{\partial^2 T}{\partial x^2}+\frac{\partial^2 T}{\partial y^2}\right) \tag{4}$$

where x and y are the spatial coordinates (m), u and v are the velocities in x and y directions (m/s), t is the time (s), ρ is the density (kg/m^3), p is the pressure (Pa), υ is the kinematic viscosity (m^2/s), T is the temperature (K) and α is the thermal diffusivity (m^2/s).

2.2. Geometrical investigation with constructal design

The application of the constructal design method in this study is illustrated in Figs. 2 and 3. In the initial steps, Fig. 2, it is crucial to define the flow system, including the domain, thermophysical properties, and boundary and initial conditions. Understanding the physical problem is essential to properly define how to facilitate the access to the internal currents (represented by maximizing/minimizing the performance indicators), the constraints, and the degrees of freedom (steps 1 to 5). Simultaneously, it is important to establish the method for solving the physical problem, which involves the numerical solution of Eqs. (1)–(4) (step 5b).

In step 3, the objectives are maximizing the average Nusselt number (Nu_D) and minimizing the average drag coefficient (C_D) in the array. The average Nu_D is given by [35]:

$$Nu_D=\frac{1}{4}\sum_{i=1}^{4}Nu_{D,i} \tag{5}$$

where the average Nusselt number for each cylinder is given by [36]:

$$Nu_{D,i}=\frac{1}{\pi D,i}\int_0^{\pi D,i}\left.\frac{\partial T^*}{\partial n^*}\right|_{n^*}d\theta \tag{6}$$

And the average C_D of the array is given by [1–2]:

$$C_D=\frac{1}{4}\sum_{i=1}^{4}\frac{2F'_{D,i}}{\rho V_\infty^2 D_i} \tag{7}$$

where i indicates the number of the cylinder ($1 \le i \le 4$), * represents the dimensionless variables, n is the normal surface to the cylinder, θ is the angle of the cylinder (rad) where the local Nusselt number is integrated, and F'_D is the drag force per unit depth (N/m).

In step 4, two constraints are defined for the problem:

- the cross-sectional areas of the cylinders

$$A_c=A_{c1}+A_{c2}+A_{c3}+A_{c4}=\pi D^2 \tag{8}$$

- the occupation area of the array

$$A_0=H_0 \bullet L_0 \tag{9}$$

where $H_0 = 6D = 0.6$ m, $L_0 = 8D = 0.8$ m, and $A_0 = 48D^2 = 0.48$ m^2.

In step 5, three degrees of freedom (DOFs) are defined: S_T/D, S_{L1}/D, and S_{L2}/D, as indicated by the dimensions in Fig. 1. Eight values of S_T/D (1.5, 2.0, 2.5, 3.0, 3.5, 4.0, 4.5, 5.0), four values of S_{L2}/D (1.5, 2.0, 2.5, 3.0) and three values of S_{L1}/D (1.5, 3.0, 4.0) are investigated. These DOFs enable the exploration of the impact of the design of the cylinder arrangement on the performance indicators. Moving to step 6, additional flow parameters are defined. Here, three distinct Reynolds numbers ($Re_D = V_\infty D/\upsilon = 10$, 40, and 150, corresponding respectively to $V_\infty = 5$ m/s, 20 m/s, and 75 m/s) are investigated. It is worth noting that it is used the similarity principle to ease the convergence of the numerical solution without any loss to the accuracy of the calculus of drag coefficient and Nusselt number. Consequently, to comprehensively address the problem, a total of 288 different cases were numerically simulated.

Fig. 3 provides a detailed depiction of the three-level flowchart outlining the geometrical investigation for each Reynolds number (step 6). In the first level, the ratio S_T/D is varied while keeping the ratios S_{L1}/D and S_{L2}/D constant. For the thermal purpose, the highest Nu_D, is the once maximized Nusselt number, $(Nu_D)_m$, and the corresponding S_T/D is the once optimized ratio of S_T/D for the thermal purpose, $(S_T/D)_{o,T}$. Similarly, for the fluid dynamic purpose, the lowest C_D is the once minimized C_D, $(C_D)_m$, and the corresponding S_T/D is the once optimized ratio of S_T/D for the fluid dynamic purpose, $(S_T/D)_{o,F}$. For the second level, the process is repeated for different ratios of S_{L2}/D while maintaining the ratio S_{L1}/D constant. The maximum Nu_D obtained is labeled as $(Nu_D)_{2m}$, and the corresponding optimal configurations are $(S_{L2}/D)_{o,T}$ and $(S_T/D)_{2o,T}$. Simultaneously, the minimum C_D is denoted as $(C_D)_{2m}$, and the corresponding optimum ratios are $(S_{L2}/D)_{o,F}$ and $(S_T/D)_{2o,F}$. The same process is applied in the third level, now varying the ratios of S_{L1}/D. The maximum Nu_D is labeled $(Nu_D)_{3m}$, the minimum C_D is denoted $(C_D)_{3m}$. The optimal ratios are presented in Fig. 3. Additionally, Fig. 3 visually represents potential optimal thermal and fluid dynamic paths, highlighted in red and blue, respectively.

After defining the search space for the geometrical investigation, Eqs. (1)–(4) are solved for each geometrical configuration (step 7, Fig. 2). Subsequently, the impacts of the degrees of freedom on both fluid dynamic and thermal performance are analyzed, along with other DOFs

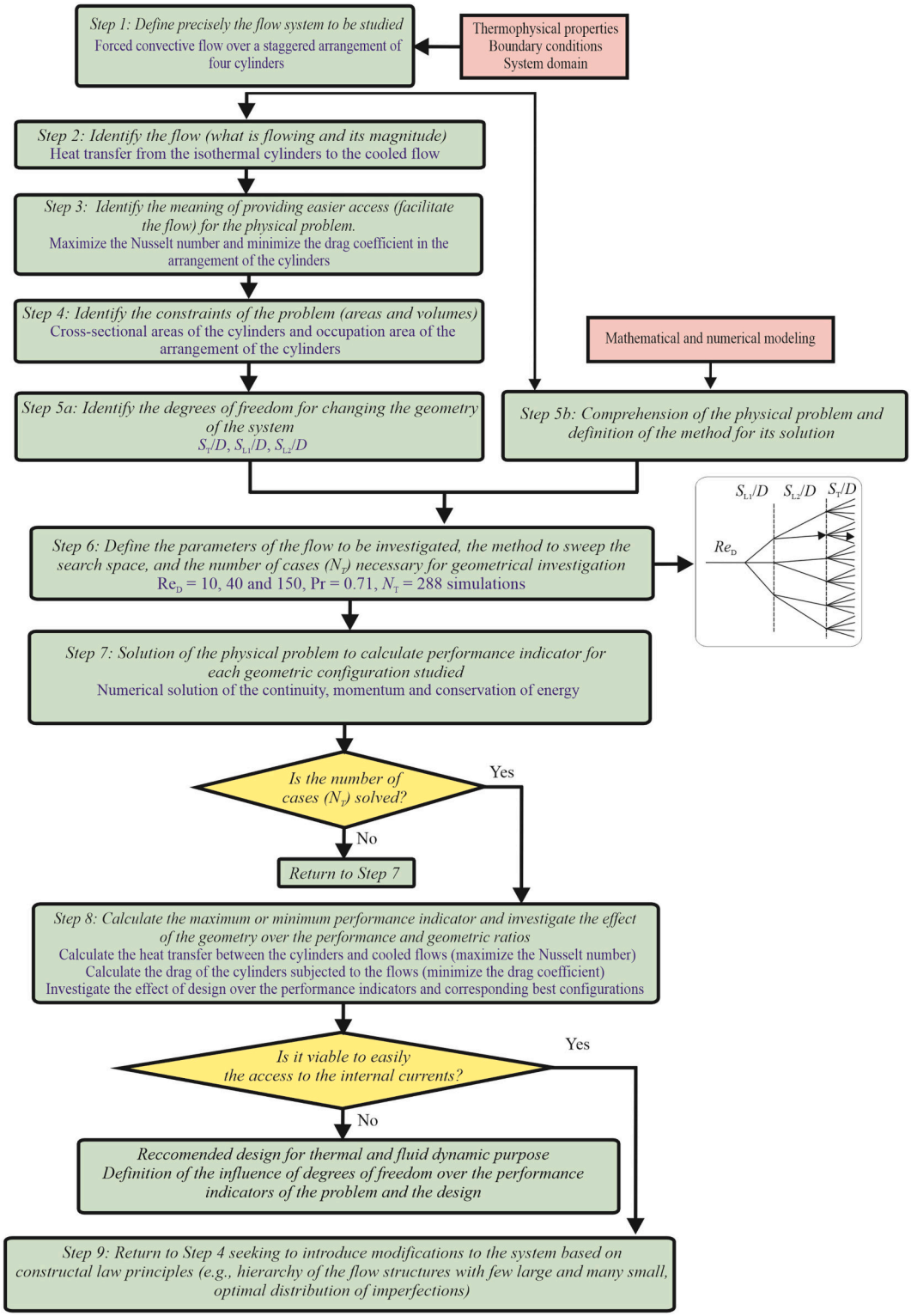

Fig. 2. Diagram of the application of constructal design for the geometrical investigation of the arrangement of cylinders subjected to forced convective flows.

(step 8). If new opportunities to facilitate the flow system are identified and deemed feasible for implementation, modifications to the system can be made based on the principles of the constructal law (step 9). In the present study, the constructal law was applied as a powerful tool to comprehend the influence of the design on the arrangement of cylinders. However, the constructal law is a much broader principle and important discussion about the principle can be found in the literature [23–25].

2.3. Numerical procedures and verification/validation of the computational method

The Eqs. (1)–(4) are numerically solved using the finite volume method (FVM), implemented in the software FLUENT, version 14 [36–38]. The numerical procedures include the utilization of the 2nd order upwind interpolation function for treating the advective terms, the semi-implicit method for pressure linked equations (SIMPLE) to handle

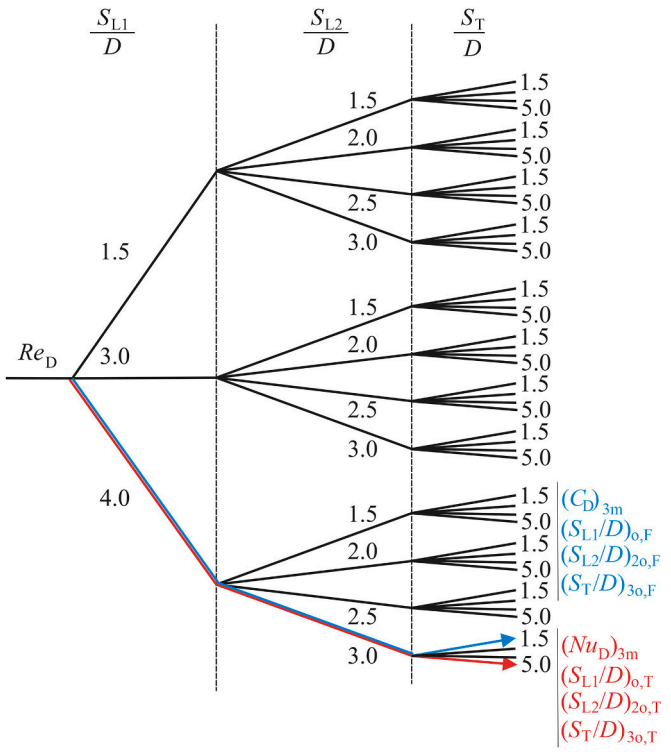

Fig. 3. Flowchart with the geometrical configurations investigated for each Reynolds number.

velocity coupling, and an implicit second-order discretization for the transient solution. Convergence in the simulations is considered achieved when the residuals of the mass, momentum, and energy equations fall below 10^{-6}, 10^{-6} and 10^{-8}, respectively. For all simulations, a physical time of $t_f = 4.0$ s is considered, with the interval 2.0 s $\leq t \leq$ 4.0 s used for obtaining time-averaged values of C_D and Nu_D. Moreover, the simulations are made using four processors (Intel) with 3.60 GHz clock and 24.0 Gb of RAM. The parallelization is performed with message passing interface (MPI) technique. For the independent mesh, the processing time for each simulation is approximately 1.8×10^3 s.

For the spatial discretization, hybrid meshes (triangular and rectangular) are generated with the software GMSH (version 3.0.6) [39]. A region with structured rectangular mesh, extending up to a diameter of 1.2 m, is implemented around the cylinders to facilitate the capture of velocity and temperature gradients in this area. Fig. 4 illustrates the hybrid mesh and the detail of the refined mesh around the cylinders. To define the mesh recommendations, a grid independence study is performed for the case $Re_D = 150$, $Pr = 0.71$, and $S_{L1}/D = S_{L2}/D = S_T/D =$ 1.5. The mesh is considered converged when the relative difference between a course and refined meshes are lower than 0.5%, as expressed by:

$$RD = 100 \bullet \left| \frac{(Nu_D^i - Nu_D^{i+1})}{Nu_D^i} \right| \leq 0.5\% \tag{10}$$

where Nu_D^i is the Nusselt number obtained with the course mesh and Nu_D^{i+1} is the Nusselt number for the next refined mesh.

Table 1 shows the results of grid independence study performed in the present work, being recommended for continuity of the study a mesh with nearly 145,282 finite volumes.

Concerning the time-dependent analysis of the problem, for $Re_D \leq 40$, the structure of fluid flow under forced convection is steady and symmetrical in the upper and lower downstream regions of one isolated cylinder. In this sense, the transient and the steady solutions led to similar fields and results for the prediction of C_D and Nu_D. As Reynolds increases to $Re_D = 150$, it is expected the arise of some unsteady and laminar structures such as von Karman vortices shedding and streets. However, this kind of flow structure is meagered for situations where surrounding walls (as the symmetry walls in the present work) have some influence on the flow around one cylinder or bundle of cylinders. For these cases, it is required higher magnitudes of Reynolds number for the generation of more complex time-dependent structures (as those reported above) or an increase of the height of the channel to a magnitude as high as $H = 75D$, as recommended in the literature [40]. For this work, the height of the computational domain is not augmented to obtain recommendations of the present arrangement for a thermal device equipment or bundle of tubes into channels subjected to any enclosure. Despite the velocity, pressure, and temperature fields being more stable and, consequently, more similar to that achieved for the steady-state solution, the later solution led to differences up to around 39% in comparison with the results of literature for the cases with one or four cylinders reported in the literature [41,42] due to inadequate prediction of velocity and temperature fields around the cylinder. Consequently, it was necessary to use the unsteady solution for adequate

Table 1
Grid independence study for the case $Re_D = 150$, $Pr = 0.71$, and $S_{L1}/D = S_{L2}/D = S_T/D = 1.5$.

Volumes	Divisions in cylinder periphery	Divisions - radial direction cylinder	Nu_D	Relative Difference - RD (%)
71,300	60	7	3.6454	7.67
84,756	90	15	3.9250	6.50
113,524	120	25	4.2101	2.65
145,282	150	40	4.3217	0.46
185,890	180	55	4.3416	

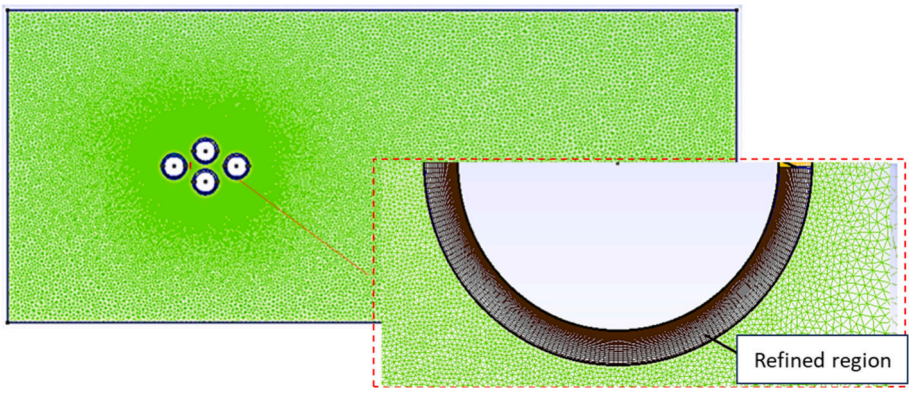

Fig. 4. Hybrid triangular and rectangular mesh used in the domain of the fluid flow with four cylinders arranged in staggered configuration.

prediction of C_D and Nu_D for $Re_D = 150$. To standardize the mathematical and numerical model throughout the investigation, the unsteady solution was also employed for the other cases of $Re_D = 10$ and 40.

To define the time-step used in the simulations, a time-step sensibility study was performed for the same case investigated in Table 1 ($Re_D = 150$, $Pr = 0.71$, $S_{L1}/D = S_{L2}/D = S_T/D = 1.5$). Table 2 illustrates the Nusselt number for the arrangement for different time-steps, considering the same criteria used for the grid-independent study. Based on the results of Table 2, a constant time-step of $\Delta t = 5.0 \times 10^{-3}$ s with 1000 iterations per time-step is employed in the present simulations.

To verify/validate the computational method, the spatial and time-averaged Nu_D for a single cylinder with $Re_D = 150$ and $Pr = 0.71$ is compared with Hilpert's correlation [41]. Furthermore, the arrangement of four cylinders, as detailed in Tables 1 and 2, is compared with Grimison's correlation [42], and the results are summarized in Table 3. Additionally, the local time-averaged Nu_D as a function of the angle for a single cylinder with $Re_D = 20$ and 200 using the present method is compared with the findings of Momose and Kimoto [43] and Bharti et al. [44], as illustrated in Fig. 5. In general, both spatial and time-averaged, and local Nusselt number exhibit good agreement with literature results, showing that the present method is suitable for the geometrical investigation conducted in this study.

3. Results and discussion

The initial investigation focuses on the impact of the ratio S_T/D on the spatial and time-averaged C_D (Fig. 6) and Nu_D (Fig. 7) for various values of the S_{L2}/D ratio and the three distinct $Re_D = 10$, 40 and 150. Throughout all cases, a constant ratio $S_{L1}/D = 1.5$ is maintained. Specifically, Figs. 6(a) and 6(b) depict a graph and an isosurface with C_D as a function of S_T/D for different S_{L2}/D values at $Re_D = 10$. Similarly, Figs. 6(c) and 6(d) exhibit similar figures for $Re_D = 40$, while Figs. 6(e) and 6(f) present the corresponding figures for $Re_D = 150$. Figs. 7(a) and 7(b) illustrate a graph and an isosurface with Nu_D as a function of S_T/D for different S_{L2}/D values at $Re_D = 10$, and Figs. 7(c) and 7(d) display analogous plots for $Re_D = 40$. Lastly, Figs. 7(e) and 7(f) illustrate similar figures for $Re_D = 150$.

Fig. 6 consistently demonstrates that an increase in the S_T/D ratio results in a proportional increase in C_D, regardless of the S_{L2}/D ratio and Re_D values. Therefore, the configurations with the smallest transversal pitches, $(S_T/D)_{o,F} = 1.5$, conducted to the optimal fluid dynamic performance for the cylinder arrangement. When comparing the optimal and worst configurations, differences of nearly 150%, 106%, and 63% are obtained, highlighting the sensitivity of the S_T/D ratio on the C_D. Additionally, some differences in C_D magnitudes are observed for different S_{L2}/D, being more evident in Figs. 6(a), 6(c), and 6(e) when $S_T/D \geq 2.5$. This behavior is corroborated in the isosurfaces presented in Figs. 6(b) – (f) for $Re_D = 10$, 40 and 150, respectively.

Fig. 7 depicts a similar influence of S_T/D on Nu_D, where Nu_D increases with the elevation in S_T/D. However, the focus here is on maximizing Nu_D. In this context, the optimal configurations are those with the intermediate cylinders positioned as far apart as possible, $(S_T/D)_{o,T} = 5.0$. The differences between the best and worst configurations are approximately 54%, 51%, and 28%, underscoring the sensitivity of the S_T/D ratio on Nu_D. Results also reveal variations in Nu_D magnitudes for different S_{L2}/D ratios. For $Re_D = 10$, the differences are more pronounced at the lowest ratios of S_T/D. As the Reynolds number increases, particularly for $Re_D = 150$, differences become more apparent in the optimal region of S_T/D, $S_T/D \geq 2.5$. It is also worth mentioning that, for $Re_D = 150$, the optimal S_T/D ratio was obtained for $(S_{L2}/D)_{o,T} = 3.0$ and $(S_T/D)_{2o,T} = 3.5$, probably by the balance between the interaction of thermal boundary layers and the momentum magnitude in the gaps around the cylinders. When compared with the triangular arrangement of cylinders studied in Barros et al. [30], the inclusion of an additional cylinder leads to a similar trend in the impact of S_T/D on C_D and Nu_D for forced convective flows, with few differences in the optimal configurations of S_T/D.

In the second level of geometrical investigation, Fig. 8 illustrates the influence of S_{L2}/D ratio on the once minimized C_D, $C_{D,m}$. The minimal C_D values obtained in Figs. 6(a), 6(c), and 6(e) are used to construct the curves for $S_{L1}/D = 1.5$ at $Re_D = 10$, 40, and 150, respectively, as shown in Figs. 8(a) – (c). The same process used to generate Fig. 6 for $S_{L1}/D = 1.5$ is repeated for the different ratios $S_{L1}/D = 3.0$ and 4.0, and the results for the optimal configurations are also used here. Fig. 8(a) indicates that, for $Re_D = 10$, an increase of S_{L2}/D leads to an augmentation of $C_{D,m}$. For $S_{L1}/D = 3.0$, a step variation is observed in the range $1.5 \leq S_{L2}/D \leq 2.0$, presenting a different behavior than noticed for the other investigated S_{L1}/D ratios. With an increase in Reynolds number to $Re_D = 40$, Fig. 8(b), the behavior of $C_{D,m}$ as a function of S_{L2}/D changes, showing a decrease of $C_{D,m}$ with an increase of S_{L2}/D. At $Re_D = 150$, Fig. 8(c), $C_{D,m}$ is insensitive to changes in S_{L2}/D for $S_{L1}/D = 1.5$ and 4.0, while for $S_{L1}/D = 3.0$, a step decrease in $C_{D,m}$ in the range $1.5 \leq S_{L2}/D \leq 2.0$ followed by a constant magnitude of $C_{D,m}$ is observed. For all Reynolds number, a step variation of $C_{D,m}$ is perceived in this range, indicating that, in this combined region with $S_{L1}/D = 3.0$ and the range $1.5 \leq S_{L2}/D \leq 2.0$, the posterior cylinder is under the influence of the fluid dynamic boundary layers of the frontal and intermediate cylinders. It is important to

Table 2
Time-step independent study for the case $Re_D = 150$, $Pr = 0.71$, and $S_{L1}/D = S_{L2}/D = S_T/D = 1.5$.

Time-step (s)	Nu_D	Relative Difference - RD (%)
Steady-state solution	2.8324	
1.0×10^{-2}	3.5457	25.18
5.0×10^{-2}	4.2114	18.77
5.0×10^{-3}	4.3217	2.62
1.0×10^{-3}	4.3265	0.11

Table 3
Comparison of results for Nu_D obtained with the present method for one and four cylinders.

Case	Nu_D – Present work	Nu_D – Literature	Difference (%)
1 cylinder	6.0388	6.2935 – Ref. [41]	4.05
4 cylinders	4.3217	4.6335 – Ref. [42]	6.73

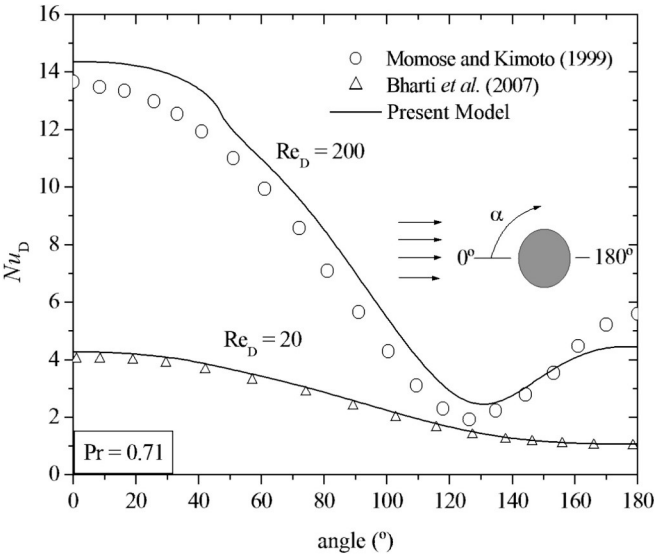

Fig. 5. Nusselt number as function of the angle of the cylinder obtained with the present computational model and results of literature for distinct Reynolds numbers ($Re_D = 20$ and $Re_D = 200$).

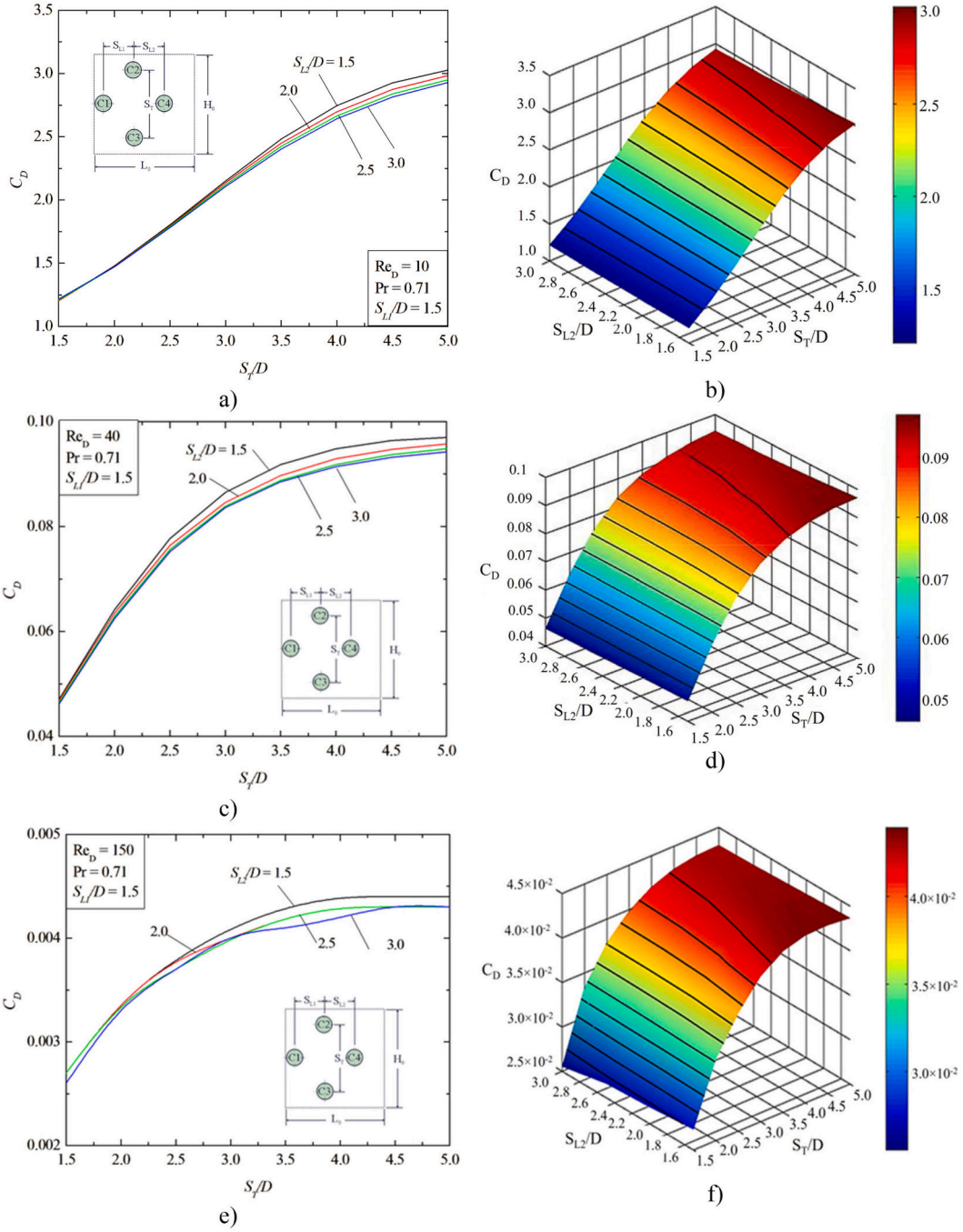

Fig. 6. Influence of the ratio S_T/D on drag coefficient (C_D) for various S_{L2}/D ratios and distinct Reynolds numbers: a) $Re_D = 10$, b) $Re_D = 10$ (isosurface), c) $Re_D = 40$, d) $Re_D = 40$ (isosurface), e) $Re_D = 150$, f) $Re_D = 150$ (isosurface). (For interpretation of the references to colour in this figure, the reader is referred to the web version of this article.)

emphasize that, regardless of S_{L1}/D and Re_D, the once optimized ratio S_T/D remained constant with $(S_T/D)_{o,F} = 1.5$. In this sense, the impact of S_{L2}/D on $(S_T/D)_{o,F}$ is not presented graphically. Despite of the lower influence of the S_{L2}/D ratio on the $C_{D,m}$ in comparison with the impact of S_T/D on C_D, differences of 3.3%, 6.7% and 13.6% are obtained for $Re_D =$ 10, 40, and 150, respectively, for a constant magnitude of S_{L1}/D.

Fig. 9 illustrates the impact of the S_{L2}/D ratio on the once maximized Nusselt number, $Nu_{D,m}$, for the investigated Reynolds numbers: $Re_D =$ 10, 40, and 150, Figs. 9(a) – (c), and the corresponding optimal ratios of $(S_T/D)_{o,T}$ for $Re_D = 150$, in Fig. 9(d). This is the only flow condition where the highest magnitude of $(S_T/D)_{o,T} = 5.0$ is not obtained. The procedure for constructing Fig. 9 is like that performed for Fig. 8. However, it is captured the highest magnitudes of Nu_D and the corresponding optimal ratios of S_T/D. For $Re_D = 10$, an increase in the S_{L2}/D ratio also conducts to an increase in $Nu_{D,m}$ for different S_{L1}/D ratios up to $S_{L2}/D = 2.5$, where the $Nu_{D,m}$ stabilizes. Moreover, the highest magnitudes of $Nu_{D,m}$ are obtained for $S_{L1}/D = 1.5$. As the Reynolds number increases, the behavior of $Nu_{D,m}$ as a function of S_{L2}/D changes. For Re_D $= 40$, $Nu_{D,m}$ increases with an increase in S_{L2}/D at $S_{L1}/D = 1.5$, whereas for $S_{L1}/D = 3.0$ and 4.0, the $Nu_{D,m}$ remains almost constant with variation of S_{L2}/D. For $Re_D = 150$, the increase in $Nu_{D,m}$ with S_{L2}/D is more perceptive for all different magnitudes of S_{L1}/D. In general, it is noticeable that S_{L2}/D has a slighter influence on the thermal performance in comparison with the effect of S_T/D on Nu_D, with variations of

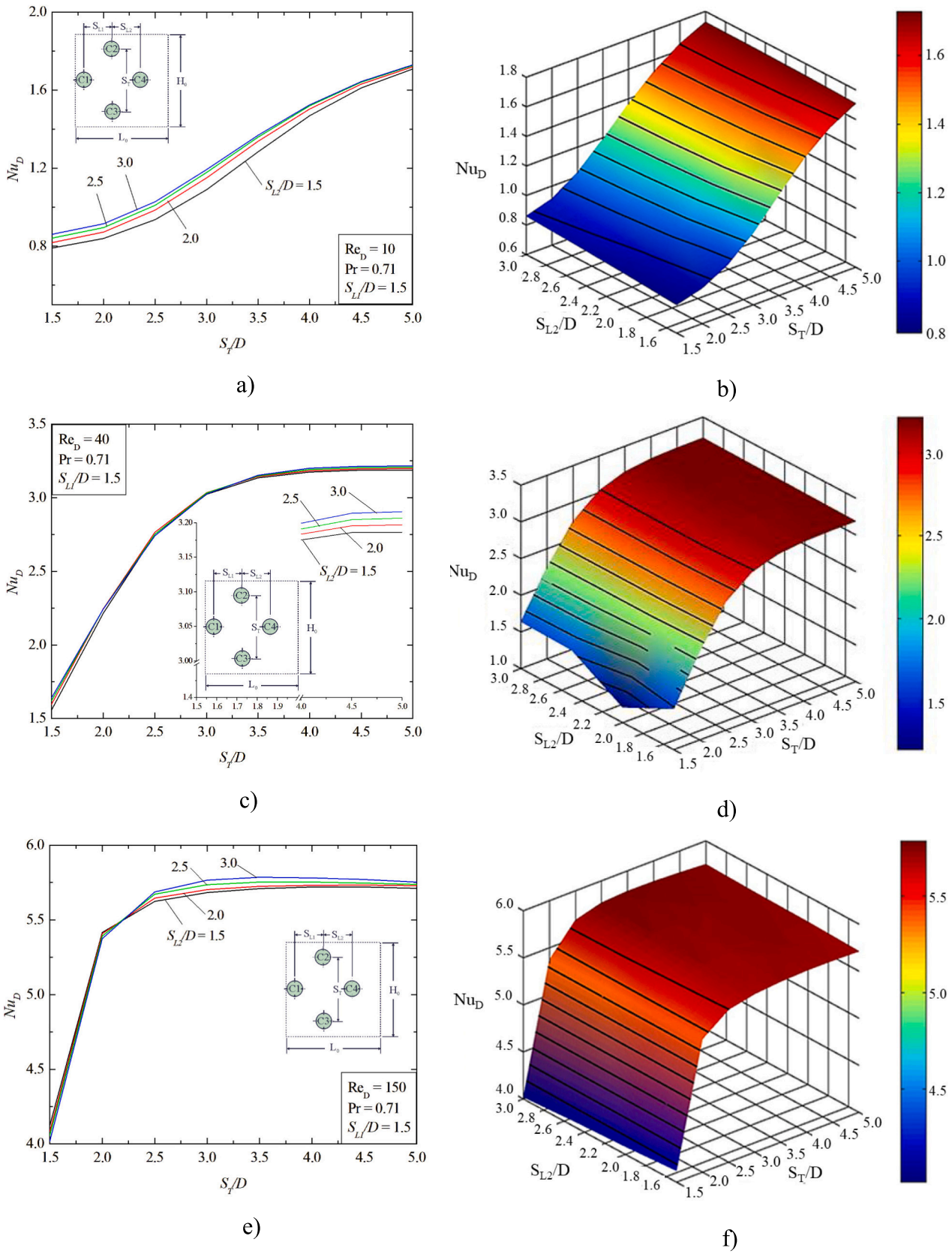

Fig. 7. Influence of the ratio S_T/D on Nusselt number (Nu_D) for various S_{L2}/D ratios and distinct Reynolds numbers: a) $Re_D = 10$, b) $Re_D = 10$ (isosurface), c) $Re_D = 40$, d) $Re_D = 40$ (isosurface), e) $Re_D = 150$, f) $Re_D = 150$ (isosurface). (For interpretation of the references to colour in this figure, the reader is referred to the web version of this article.)

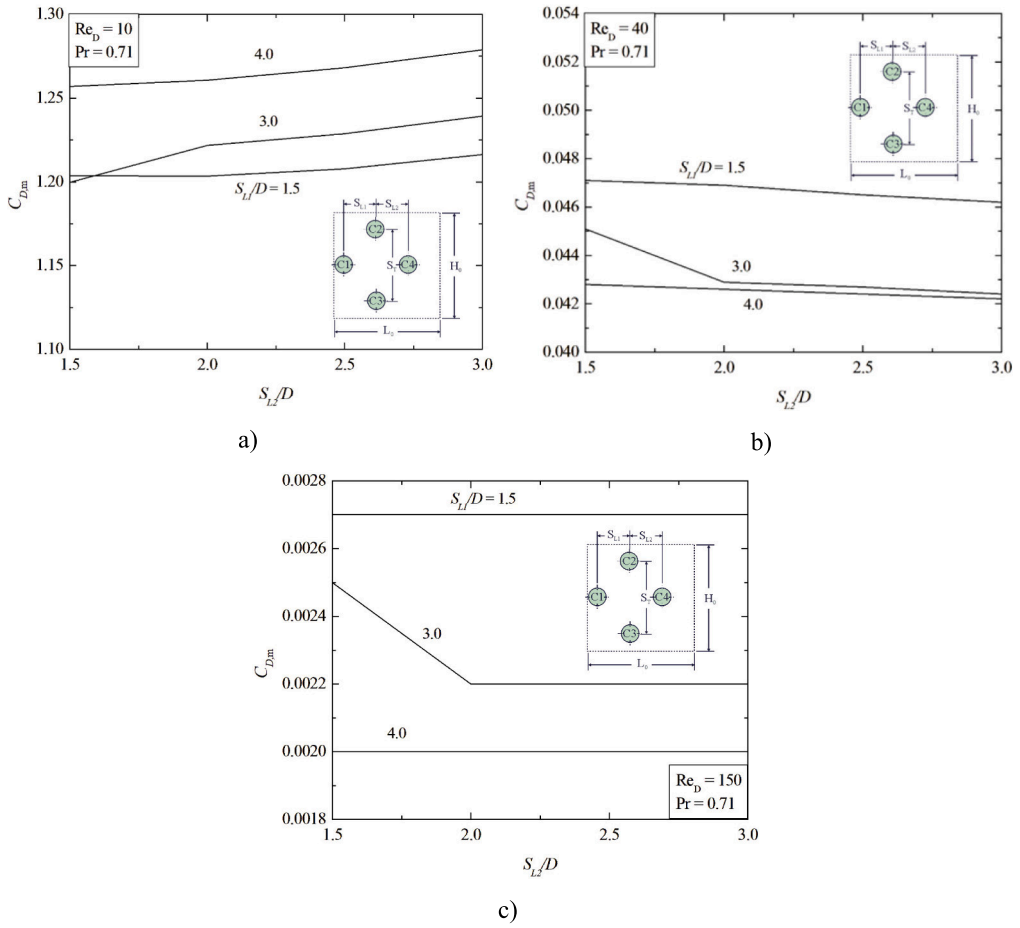

Fig. 8. Influence of the ratio S_{L2}/D on the once minimized drag coefficient, $C_{D,m}$, for various S_{L1}/D and distinct Re_D: a) $Re_D = 10$, b) $Re_D = 40$, c) $Re_D = 150$.

1.2%, 0.9%, and 1.2% in the $Nu_{D,m}$, for $Re_D = 10$, 40, and 150, respectively. Despite that, it is worth mentioning that one additional area of heat exchange is being included in comparison with a triangular arrangement of cylinders, for example, being an advantage in comparison with this previous studied array. Moreover, the effect of the ratio S_{L2}/D on $Nu_{D,m}$ changes with variation in the Reynolds number. For the lowest Reynolds, it is noticed a proximity between the frontal and intermediate cylinders, seeking to increase the momentum between the cylinders and the posterior cylinder more apart from the group of three cylinders. For the highest Reynolds, the flow intensity increases, and the increase of longitudinal pitches becomes advantageous for the thermal performance. Fig. 9(d) shows that the influence of the ratio S_{L2}/D over the $(S_T/D)_{o,T}$ depends on the magnitude of the S_{L1}/D ratio. For $S_{L1}/D = 1.5$, an increase from $S_{L2}/D = 1.5$ to 2.0 decreases the resistance to flow in the array gap, leading to an increase in S_T/D. As the ratio S_{L2}/D increases further, the space among the cylinders increases, and the transversal pitch decreases again to augment the momentum in the region among the first three cylinders. For the other ratios of S_{L1}/D, once the first cylinder is distant from the intermediate cylinders, the departure of the posterior cylinder makes the distribution of the thermal boundary layer the main responsible for thermal performance. Then, the increase of S_{L2}/D conducts to an increase of $(S_T/D)_{o,T}$.

In the third level of geometrical investigation for fluid dynamic performance, the influence of the S_{L1}/D ratio on the twice minimized drag coefficient, $C_{D,2m}$, and the corresponding optimal configurations, $(S_{L2}/D)_{o,F}$ and $(S_T/D)_{2o,F}$, are investigated. Figs. 10(a) – (c) illustrate this effect for $Re_D = 10$, 40, and 150, respectively. Irrespective of the Reynolds number, the results demonstrate that the ratio $(S_T/D)_{2o,F}$ remains insensitive to variation of S_{L1}/D, and the best performances are consistently achieved for the lowest magnitudes of $(S_T/D)_{2o,F} = 1.5$, i.e., as close as possible. For $Re_D = 10$, Fig. 10(a), the magnitude of $C_{D,2m}$ is nearly constant, with a slight drop in the range $1.5 \leq S_{L1}/D \leq 3.0$, followed by an increase for $S_{L1}/D \geq 3.0$. The best configuration was attained for $(S_{L1}/D)_{o,F} = 3.0$, with the difference between the best and worst performance being approximately 5.0%. Results also reveal that the ratio $(S_{L2}/D)_{o,F}$ decreases from $(S_{L2}/D)_{o,F} = 2.0$ to $(S_{L2}/D)_{o,F} = 1.5$ when S_{L1}/D varies from 1.5 to 3.0, indicating a tendency of the posterior longitudinal pitch to compensate the increase in the frontal pitch, preventing a spread of the array in the occupation area, given the low flow intensity. For $Re_D = 40$ and 150, as shown in Figs. 10(b) and 10(c), the influence of the S_{L1}/D ratio on the $C_{D,2m}$ and the optimal ratios is quite similar. The $C_{D,2m}$ decreases, and the ratios $(S_T/D)_{2o,F}$ and $(S_{L2}/D)_{o,F}$ remain insensitive to the increase of the ratio S_{L1}/D. The difference between the best and worst configurations is 9.5% and 35% for $Re_D = 40$ and 150, respectively.

For thermal purposes, Fig. 11 shows the impact of the S_{L1}/D ratio on the twice-maximized Nusselt number, $Nu_{D,2m}$, and the corresponding optimal configurations, $(S_{L2}/D)_{o,T}$ and $(S_T/D)_{2o,T}$, for three distinct Reynolds numbers: $Re_D = 10$, 40, and 150. In the case of $Re_D = 10$, Fig. 11(a), the results demonstrate that an increase in S_{L1}/D leads to a decrease of $Nu_{D,2m}$, suggesting that the optimal thermal arrangement occurs when the upstream and intermediate cylinders are closely aligned in the longitudinal direction. It is also noticed the optimal transversal pitch remains constant at $(S_T/D)_{2o,T} = 5.0$ for all values of S_{L1}/D, i.e., reflecting the furthest separation in the transversal direction due to the interaction between the thermal boundary layers. Additionally, $(S_{L2}/D)_{o,T} = 3.0$ is obtained in the optimal region of S_{L1}/D, indicating that the posterior cylinder is farther apart from the other three cylinders in the flow direction. Moreover, in the range $3.0 \leq S_{L1}/D \leq 4.0$, there is a slight decrease to $(S_{L2}/D)_{o,T} = 2.5$. For $Re_D = 40$, Nu_D shows a

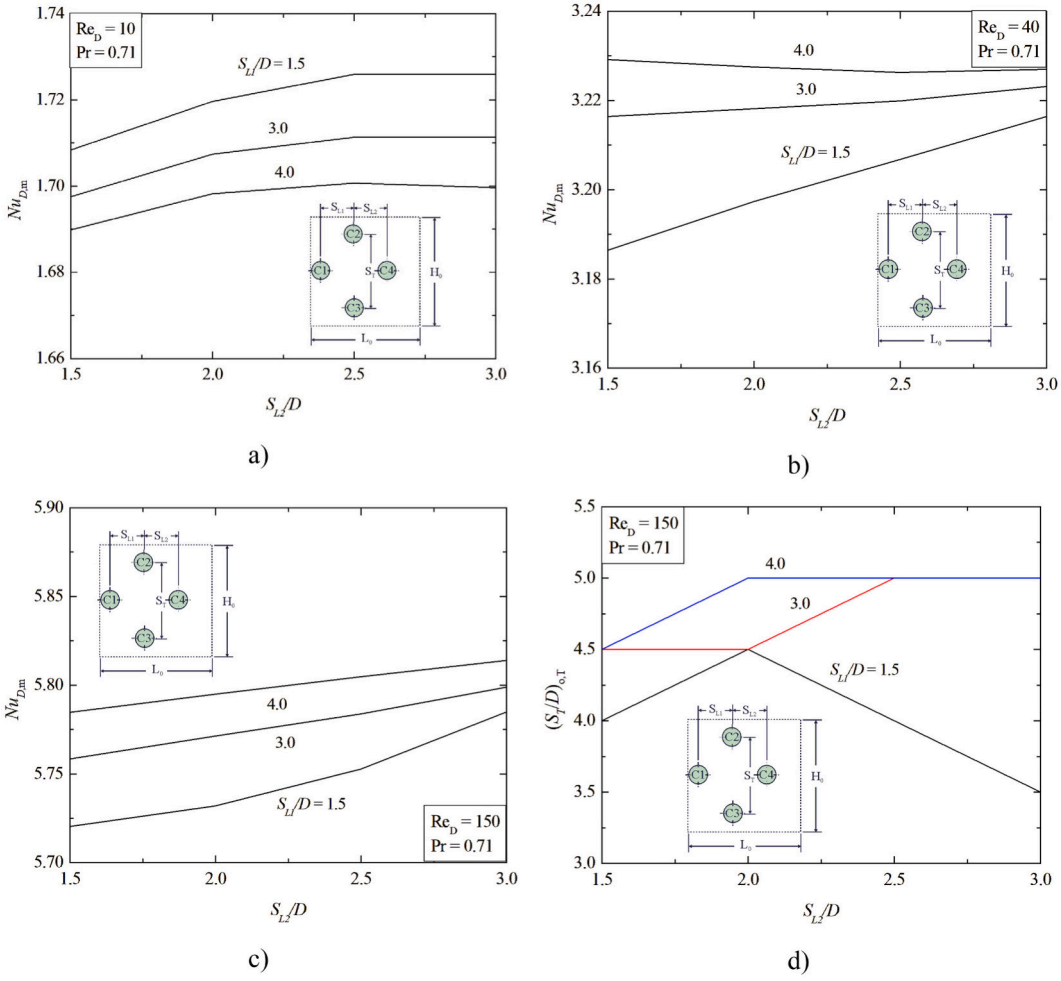

Fig. 9. Influence of the ratio S_{L2}/D on the once maximized Nusselt number, $Nu_{D,m}$, for various S_{L1}/D and distinct Re_D: a) $Re_D = 10$, b) $Re_D = 40$, c) $Re_D = 150$, and d) corresponding optimal configuration for $(S_T/D)_{o,F}$ with $Re_D = 150$. (For interpretation of the references to colour in this figure, the reader is referred to the web version of this article.)

slight increase with S_{L1}/D ratio, unlike the behavior noticed for $Re_D = 10$. In this case, the optimal configuration suggests an increased distance between the upstream and intermediate cylinders. Furthermore, the ratio $(S_T/D)_{2o,T}$ remains insensitive to variations in the S_{L1}/D ratio, while the ratio $(S_{L2}/D)_{o,T} = 3.0$ is obtained in the range $1.5 \leq S_{L1}/D \leq 3.0$, followed by a decrease to $(S_{L2}/D)_{o,T} = 1.5$ in the optimal region of $S_{L1}/D = 4.0$. For $Re_D = 40$, the intermediate cylinders are close to the downstream cylinder. In the case of $Re_D = 150$, Fig. 11(c), $Nu_{D,2m}$ increases with the augmentation of S_{L1}/D, exhibiting a similar behavior to that observed for $Re_D = 40$. However, for the $Re_D = 150$, $(S_T/D)_{2o,T}$ differs from the maximum magnitude in the range $1.5 \leq S_{L1}/D \leq 3.0$, and a constant magnitude of $(S_{L2}/D)_{o,T} = 3.0$ is obtained for all values of S_{L1}/D. Therefore, the optimal configuration for $Re_D = 150$ spreads along all the entire occupation area, a behavior not observed for the configurations with $Re_D = 10$ and 40.

Finally, Figs. 12 and 13 illustrate the impact of Re_D on the three times minimized drag coefficient, $C_{D,3m}$, Nusselt number three times maximized, $Nu_{D,3m}$, and the corresponding optimal configurations for both performance indicators, $(S_{L1}/D)_o$, $(S_{L2}/D)_{2o}$ and $(S_T/D)_{3o}$, respectively. Additionally, Fig. 12(b) depicts the pressure and velocity fields obtained when the flow reaches the steady state for the optimal fluid dynamics configurations, while Fig. 13(b) illustrates the thermal fields obtained at the steady state for the optimal thermal configurations.

For fluid dynamic purposes, Fig. 12(a) shows a step decrease in $C_{D,3m}$ from $Re_D = 10$ to $Re_D = 40$, followed by a gradual decrease in the range $40 \leq Re_D \leq 150$. This behavior aligns with expectations, resembling that observed for a single cylinder. Regarding the optimal configurations, asymmetrical patterns in the longitudinal direction are evident for all investigated Reynolds numbers for the present conditions, with $(S_{L1}/D)_{o,F} \neq (S_{L2}/D)_{2o,F}$. Moreover, in all range of Re_D examined, the upstream pitch (S_{L1}) consistently exhibited a higher magnitude than the downstream pitch (S_{L2}). This suggests that the use of variable pitches in the flow direction can enhance the fluid dynamic performance of the system. It is also observed that the optimal ratio $(S_T/D)_{3o,T}$ remained constant and at the lowest magnitude irrespective of Re_D. In the case $Re_D = 10$, the optimal arrangement was reached for $(S_{L1}/D)_{o,F} = 3.0$, $(S_{L2}/D)_{2o,F} = 1.5$, and $(S_T/D)_{3o,F} = 1.5$, indicating the upstream cylinder is farther from the intermediate cylinders, while the three posterior cylinders are as close to each other as possible. As Re_D increases to 40 and 150, the arrangement extends in the longitudinal direction, maintaining the asymmetrical pattern. Furthermore, the best configurations are those that effectively distribute the pressure difference between the frontal and posterior regions of the arrangements, as seen in Fig. 12(b). These behaviors align with the principles of constructal law, as systems of higher magnitudes tend to be larger in size than flow systems of lower magnitudes, and the design in flow systems aims to distribute the imperfections in the most homogeneous manner possible.

For the thermal purposes, Fig. 13(a) illustrates a step increase in $Nu_{D,3m}$ in the range $10 \leq Re_D \leq 40$, followed by a smoother growth for $Re_D \geq 40$, as expected. Similar to the analysis of $C_{D,3m}$, the behavior observed here also resembles the influence of Re_D on Nu_D for a single cylinder. Regarding the optimal configurations, the ratio $(S_T/D)_{3o,T}$

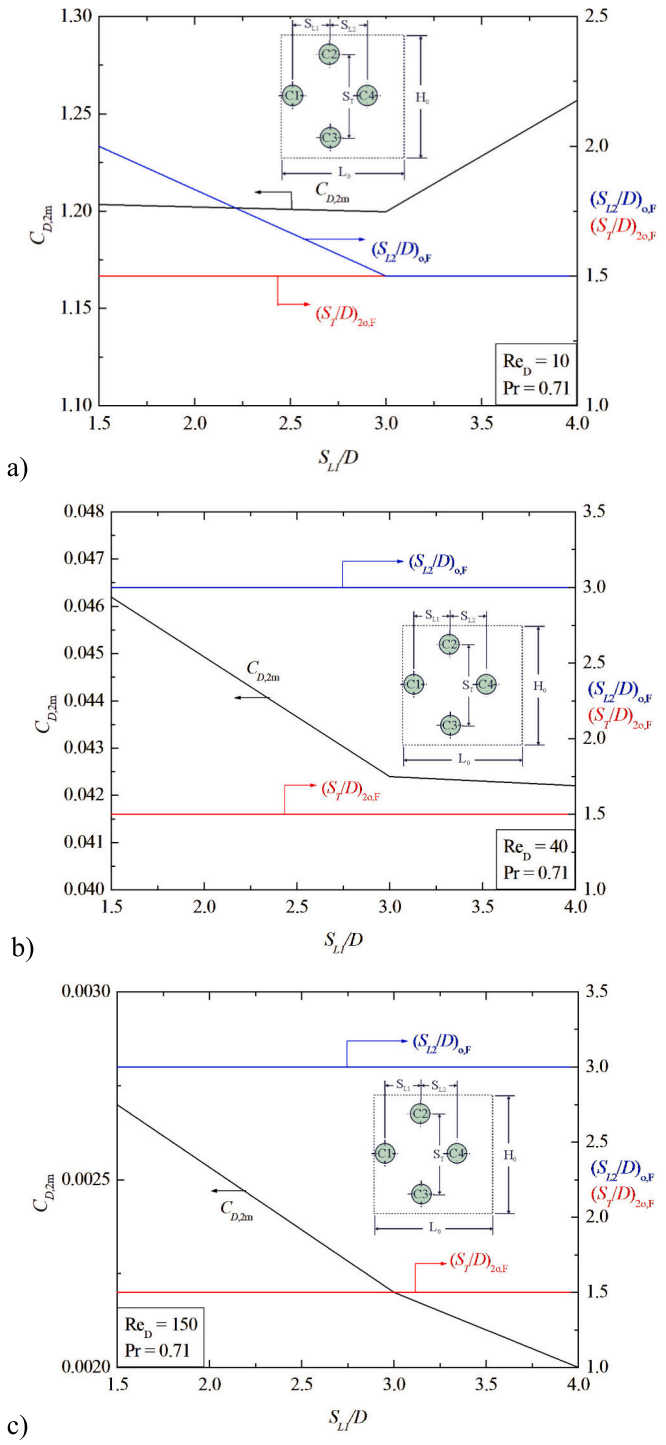

Fig. 10. Influence of the ratio S_{L1}/D on the twice minimized drag coefficient, $C_{D,2m}$, and the corresponding optimal configurations for distinct Reynolds numbers: a) $Re_D = 10$, b) $Re_D = 40$, c) $Re_D = 150$. (For interpretation of the references to colour in this figure, the reader is referred to the web version of this article.)

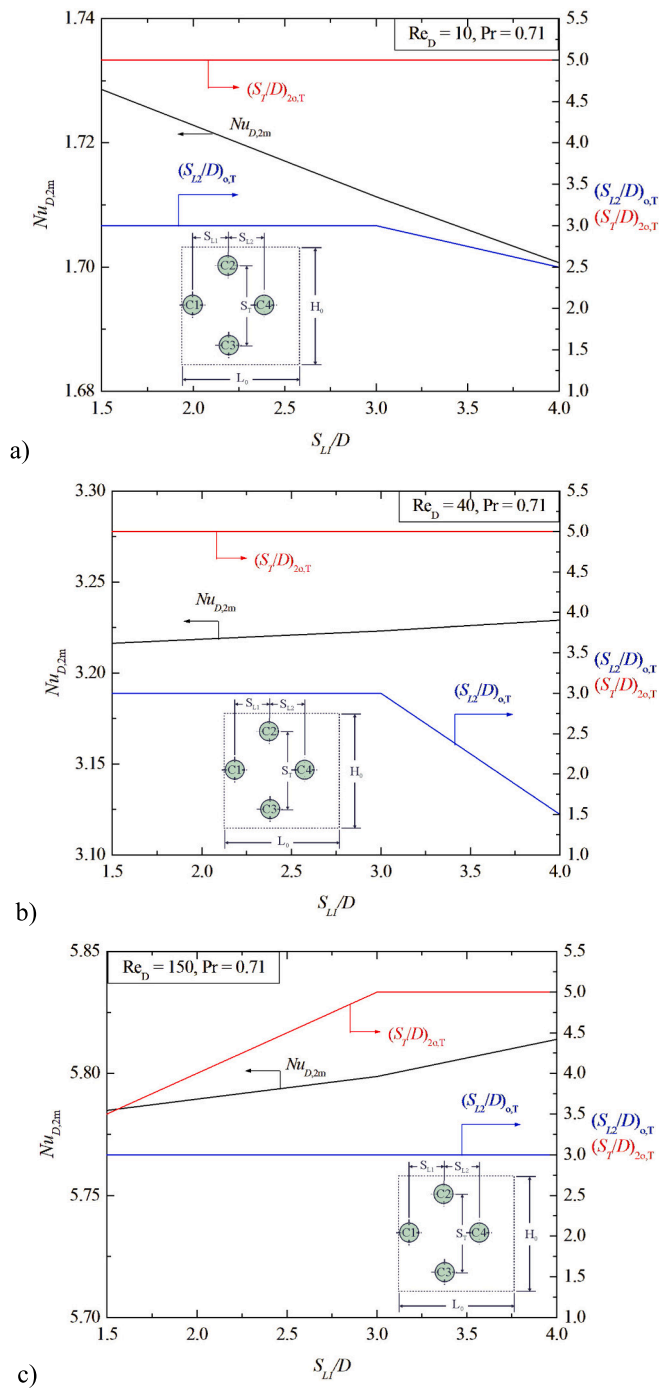

Fig. 11. Influence of the ratio S_{L1}/D on the twice maximized Nusselt number, $Nu_{D,2m}$, and the corresponding optimal configurations for distinct Re_D: a) $Re_D = 10$, b) $Re_D = 40$, c) $Re_D = 150$. (For interpretation of the references to colour in this figure, the reader is referred to the web version of this article.)

remained constant and as distant as possible for the entire range of Re_D, i.e., $(S_T/D)_{3o,T} = 5.0$. For the longitudinal pitches, asymmetrical configurations outperformed symmetrical ones for the present conditions. For $Re_D = 10$, the proximity of the upstream and intermediate cylinders enhances momentum in the gap between the cylinders, while the downstream cylinder is positioned farther apart to mitigate the impact of the thermal boundary layers from the upstream cylinders. As Re_D increases to 40, the ratio $(S_{L1}/D)_{o,T}$ undergoes a step increase from 1.5 to 4.0. This change can be explained by the increase of momentum between the cylinders, rendering it unnecessary for the first cylinders to be as close as possible. Consequently, the intermediate cylinders shift toward the downstream cylinder. However, the flow intensity is insufficient to extend the posterior cylinder as well. The expansion of the arrangement is observed for $Re_D = 150$, where it spans over the entire occupation area. Notably, an increase in $(S_{L2}/D)_{2o,T}$ is observed in the range $40 \leq Re_D \leq 150$, suggesting that the restriction imposed by the occupation area prevents the generation of a symmetrical pattern for

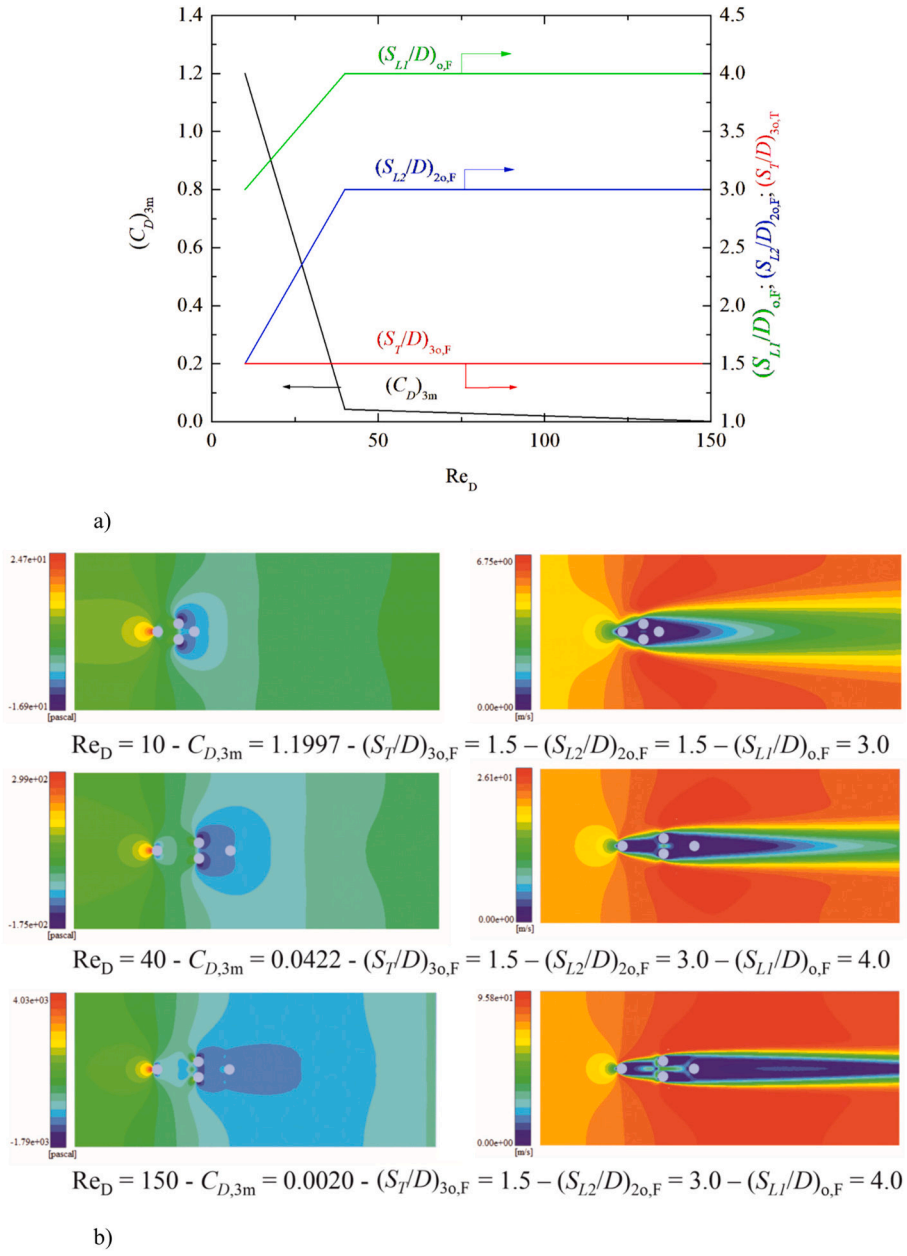

Fig. 12. Influence of the Reynolds number on: a) the three times minimized drag coefficient, ($C_{D,3m}$), and the corresponding optimal configurations, b) optimal pressure and velocity fields.

this flow condition (Re_D = 150), or indicating a tendency to obtain symmetrical patterns for higher Reynolds numbers. Despite this, under the present conditions, asymmetrical configurations conducted to the best fluid dynamic and thermal performances, and the use of varied longitudinal pitches along the flow stream showed promise as a strategic approach. The results for the thermal fields reinforce that flow systems of low magnitude tend to generate smaller configurations, and as the intensity of the flow system increases, large configurations emerge. Moreover, the generated designs followed the constructal law principles. Results also indicated that the use of a sort of strategy to modify the arrangement as a function of time and operation conditions can also benefit the system.

To compare the optimal configurations for fluid-dynamic and thermal purposes to each other, the obtained values of both drag coefficient and Nusselt number are reported for each optimized arrangement of cylinders. In detail, with Re_D = 10, 40, and 150, the optimal configurations for fluid dynamic purposes lead respectively to Nu_D = 0.8214, 1.7468, and 3.6737, which are 52.48%, 45.90%, and 36.81% lower than the Nusselt values obtained by the corresponding optimal configurations for thermal purposes (Nu_D = 1.7286, 3.2291, and 5.8140, respectively). On the other hand, with Re_D = 10, 40, and 150, the optimal configurations for thermal purposes lead respectively to C_D = 2.9295, 0.0943, and 0.0041, which are 144.19%, 123.46%, and 105.00% lower than the drag coefficient values obtained by the corresponding optimal configurations for fluid dynamic purposes (C_D = 1.1997, 0.0422, and 0.0020, respectively).

4. Conclusions

The present numerical work explored the configuration of a staggered arrangement of four cylinders using a constructal design approach. The problem is constrained by the areas of the cylinders and occupation area of the arrangement, and it involves three degrees of freedom (S_T/D, S_{L2}/D, and S_{L1}/D). This setup enabled an examination

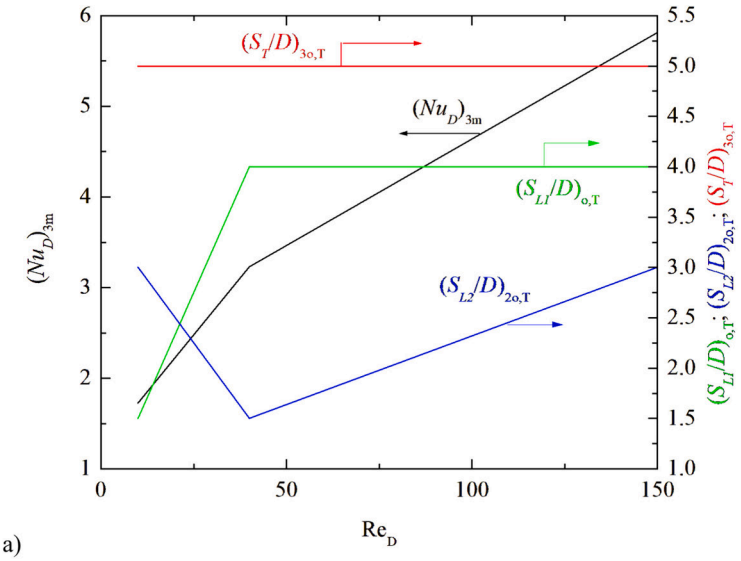

a)

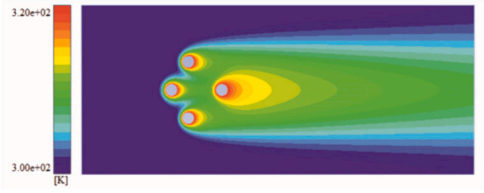

$Re_D = 10$ - $Nu_{D,3m} = 1.7286$ - $(S_T/D)_{3o,T} = 5.0$ – $(S_{L2}/D)_{2o,T} = 3.0$ – $(S_{L1}/D)_{o,T} = 1.5$

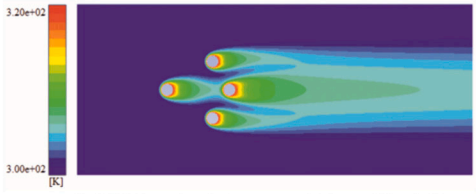

$Re_D = 40$ - $Nu_{D,3m} = 3.2291$ - $(S_T/D)_{3o,T} = 5.0$ – $(S_{L2}/D)_{2o,T} = 1.5$ – $(S_{L1}/D)_{o,T} = 4.0$

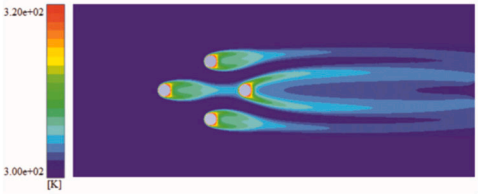

$Re_D = 150$ - $Nu_{D,3m} = 5.8140$ - $(S_T/D)_{3o,T} = 5.0$ – $(S_{L2}/D)_{2o,T} = 3.0$ – $(S_{L1}/D)_{o,T} = 4.0$

b)

Fig. 13. Influence of the Reynolds number on: a) the three times maximized Nusselt number, $Nu_{D,3m}$, and the corresponding optimal configurations, b) optimal temperature fields.

about the potential advantages in employing varied longitudinal pitches for both fluid dynamic and thermal performances of the arrangement. The geometrical investigation was conducted by varying different Reynolds numbers (Re_D = 10, 40, and 150) while maintaining a constant Prandtl number (Pr = 0.71).

The results provided significant insights and recommendations for the design of the arrangement of cylinders concerning their fluid dynamic and thermal performances, measured by the drag coefficient (C_D) and Nusselt number (Nu_D). Overall, the lowest and highest magnitudes of transversal pitches (S_T/D) lead to the best fluid dynamic and thermal performances. In particular, comparing the optimal and worst configurations for fluid dynamic (thermal) purposes, differences up to 150% (54%) on the C_D (Nu_D) value were obtained by varying the value of S_T/D. Notably, the transversal pitch (S_T/D) exhibited greater sensitivity in the performance compared to longitudinal pitches, irrespective of the Reynolds number (Re_D) under investigation. Indeed, differences up to 13.6% were obtained in the value of $C_{D,m}$, and up to 1.2% in the value of $Nu_{D,m}$, by varying the S_{L2}/D ratio. In addition, the variations in the value of S_{L1}/D led to differences of up to 35% in the value of $C_{D,2m}$, and up to 5.2% in the value of $Nu_{D,2m}$.

Despite their lower influence compared to S_T/D, longitudinal pitches made significant contributions to minimizing C_D and maximizing Nu_D. The results also indicated that employing different pitches (S_{L1}/D, and S_{L2}/D) could be an effective strategy for enhancing the fluid dynamic and thermal performance of the array. This observation was supported by the achievement of asymmetrical optimal configurations for all investigated Reynolds numbers. Furthermore, the results showed a strong dependence of the arrangement configuration on Reynolds

number. For fluid flows of low intensity, represented by $Re_D = 10$, the optimal configurations for fluid dynamic ($(S_T/D)_{3o,F} = 1.5$, $(S_{L2}/D)_{2o,F} = 1.5$, $(S_{L1}/D)_{o,F} = 3.0$) and thermal purposes ($(S_T/D)_{3o,T} = 5.0$, $(S_{L2}/D)_{2o,T} = 3.0$, $(S_{L1}/D)_{o,T} = 1.5$) tend to be as small as possible. As the flow intensity increased to $Re_D = 40$ and 150, the arrangement expanded, using more space within the occupation area: $(S_T/D)_{3o,F} = 1.5$, $(S_{L2}/D)_{2o,F} = 3.0$, $(S_{L1}/D)_{o,F} = 4.0$ and $(S_T/D)_{3o,T} = 5.0$, $(S_{L2}/D)_{2o,T} = 1.5$, $(S_{L1}/D)_{o,T} = 4.0$ for $Re_D = 40$; $(S_T/D)_{3o,F} = 1.5$, $(S_{L2}/D)_{2o,F} = 3.0$, $(S_{L1}/D)_{o,F} = 4.0$ and $(S_T/D)_{3o,T} = 5.0$, $(S_{L2}/D)_{2o,T} = 3.0$, $(S_{L1}/D)_{o,T} = 4.0$ for $Re_D = 150$. In particular, in the thermal arrangement with $Re_D = 150$, where the highest S_T/D led to the best thermal performance, the optimal thermal arrangement spanned over the entire occupation area. In general, the optimal configurations were those that distributed imperfections in the most homogeneous manner possible, in accordance with the constructal law.

In future works, it is recommended to explore constraints related to other occupation areas, consider higher Reynolds numbers and other working fluids, and extend the study to convective flows under different conditions, such as the simulation of mixed convective cases. These investigations can provide an even greater comprehension of the influence of the design of cylinder' arrays under various scenarios. It is also recommended to develop a sort of transient control of the arrangement to improve its fluid dynamic and thermal performance.

CRediT authorship contribution statement

Ana Paula Del Aghenese: Visualization, Validation, Software. **Claudia Naldi:** Writing – review & editing, Methodology, Investigation. **Luiz Alberto Oliveira Rocha:** Supervision, Funding acquisition. **Liércio André Isoldi:** Visualization, Validation, Software, Data curation. **João Francisco Prolo Filho:** Validation, Software, Formal analysis, Data curation. **Cesare Biserni:** Writing – review & editing, Resources. **Elizaldo Domingues dos Santos:** Writing – review & editing, Writing – original draft, Supervision, Methodology, Investigation, Conceptualization.

Declaration of competing interest

The authors declare that they have no known competing financial interests or personal relationships that could have appeared to influence the work reported in this paper.

Data availability

Data will be made available on request.

Acknowledgements

A.P. Del Aghnese thanks CAPES - Coordination for the Improvement of Higher Education Personnel for the master scholarship (Finance Code 001). L.A.O. Rocha, L.A. Isoldi, and E.D. dos Santos thank CNPq – National Council of Scientific and Technological Development for the research grant (Processes: 307791/2019-0, 309648/2021-1, 308396/2021-9). Authors also thank FAPERGS – *Fundação de Apoio à Pesquisa do Estado do Rio Grande do Sul* (Grant number: 19/2551-0001847-9). C. Biserni and C. Naldi are sponsored by the National Recovery and Resilience Plan (NRRP), Mission 4 Component 2 Investment 1.5 - Call for tender No. 3277 of 30/12/2021 of Italian Ministry of University and Research funded by the European Union – NextGenerationEU; project code ECS00000033, Concession Decree No. 1052 of 23/06/2022 adopted by the Italian Ministry of University and Research, CUP D93C22000460001, "Ecosystem for Sustainable Transition in Emilia-Romagna" (Ecosister), Spoke 4.

References

[1] M.M. Zdravkovich, Flow Around Circular Cylinders Vol. 1: Fundamentals, Oxford University Press, 1997.
[2] M.M. Zdravkovich, Flow Around Circular Cylinders Vol. 2: Applications, Oxford University Press, 2003.
[3] D. Sumner, Two circular cylinders in cross-flow: a review, J. Fluid. Struct. 26 (2010) 849–899, https://doi.org/10.1016/j.jfluidstructs.2010.07.001.
[4] S.-L. Cao, X. Sun, J.-Z. Zhang, Y.-X. Zhang, Forced convection heat transfer around a circular cylinder in laminar flow: an insight from Lagrangian coherent structures, Phys. Fluids 33 (6) (2021) 067104, https://doi.org/10.1063/5.0049219.
[5] R. Pravesh, A. Dhiman, R.P. Bharti, Thermal features of mixed convection from an inline periodic array of circular cylinders in non-Newtonian power-law fluids, Case Stud. Therm Eng. 36 (2022) 102175, https://doi.org/10.1016/j.csite.2022.102175.
[6] M. Islam, S. Kumar, Y.Y. Fatt, I. Janajreh, Flow-induced vibration and heat transfer in arrays of cylinders: effects of transverse spacing and cylinder diameter, Int. Commun. Heat Mass Transf. 149 (2023) 107159, https://doi.org/10.1016/j.icheatmasstransfer.2023.107159.
[7] S. Li, T. Zhou, Z. Sun, Z. Dong, External forced convection from circular cylinders with surface protrusions, Int. J. Heat Mass Transf. 99 (2016) 20–30, https://doi.org/10.1016/j.ijheatmasstransfer.2016.03.092.
[8] S. Bouzari, J. Ghazanfarian, Unsteady forced convection over cylinder with radial fins in cross flow, Appl. Therm. Eng. 112 (2017) 214–225, https://doi.org/10.1016/j.applthermaleng.2016.10.052.
[9] X. Sun, Z. Ye, J. Li, K. Wen, H. Tian, Forced convection heat transfer from a circular cylinder with a flexible fin, Int. J. Heat Mass Transf. 128 (2019) 319–334, https://doi.org/10.1016/j.ijheatmasstransfer.2018.08.123.
[10] S. Iousef, H. Montazeri, B. Blocken, P.J.V. van Wesemael, Wall-resolved versus wall-modeled LES of the flow field and surface forced convective heat transfer for a low-rise building, Build. Environ. 244 (2023) 110678, https://doi.org/10.1016/j.buildenv.2023.110678.
[11] A. Kumar, A. Dhiman, L. Baranyi, Fluid flow and heat transfer around a confined semi-circular cylinder: onset of vortex shedding and effects of Reynolds and Prandtl numbers, Int. J. Heat Mass Transf. 102 (2016) 417–425, https://doi.org/10.1016/j.ijheatmasstransfer.2016.06.026.
[12] S. Chamoli, T. Tang, P. Yu, R. Lu, Effect of shape modification on heat transfer and drag for fluid flow past a cam-shaped cylinder, Int. J. Heat Mass Transf. 131 (2019) 1147–1163, https://doi.org/10.1016/j.ijheatmasstransfer.2018.11.057.
[13] H.S. Yoon, S.H. Nam, M.I. Kim, Laminar forced convection heat transfer around wavy elliptic cylinders with different aspect ratios, Int. J. Heat Mass Transf. 194 (2022) 123038.
[14] H.S. Yoon, J. Moon, Effect of variable pitch on forced convection heat transfer around a helically twisted elliptic cylinder, Int. J. Heat Mass Transf. 173 (2021) 121205, https://doi.org/10.1016/j.ijheatmasstransfer.2021.121205.
[15] M.R. Lekkala, M. Latheef, J.H. Jung, A. Coraddu, H. Zhu, N. Srinil, B.-H. Lee, D. K. Kim, Recent advances in understanding the flow over bluff bodies with different geometries at moderate Reynolds numbers, Ocean Eng. 261 (2022) 111611, https://doi.org/10.1016/j.oceaneng.2022.111611.
[16] Z. Wang, S. Zu, M. Yang, Numerical simulation on forced convection over a circular cylinder confined in a sudden expansion channel, Int. Commun, Heat Mass Transf. 91 (2018) 48–56, https://doi.org/10.1016/j.icheatmasstransfer.2017.11.005.
[17] F.S. Oğlakkaya, C. Bozkaya, MHD forced convection flow in an infinite channel with a rotating cylinder, Eng. Anal. Bound. Elem. 156 (2023) 189–198, https://doi.org/10.1016/j.enganabound.2023.07.045.
[18] D. Ambesi, C.R. Kleijn, Laminar forced convection heat transfer to ordered and disordered single rows of cylinders, Int. J. Heat Mass Transf. 55 (2012) 6170–6180, https://doi.org/10.1016/j.ijheatmasstransfer.2012.06.038.
[19] L. Daróczy, G. Janiga, D. Thévenin, Systematic analysis of the heat exchanger arrangement problem using multi-objective genetic optimization, Energy 65 (2014) 364–373, https://doi.org/10.1016/j.energy.2013.11.035.
[20] R. Pravesh, A. Dhiman, R.P. Bharti, Thermal features of mixed convection from an inline periodic array of circular cylinders in non-Newtonian power-law fluids, Case Stud. Therm. Eng. 36 (2022) 102175, https://doi.org/10.1016/j.csite.2022.102175.
[21] J. Xue, R. Zhao, D. Zhang, R. Cheng, Numerical optimization of forced thermal convection in transverse tube bundles based on double-distribution-function lattice Boltzmann method, Case Stud. Therm. Eng. 51 (2023) 103604, https://doi.org/10.1016/j.csite.2023.103604.
[22] Md. Islam, S. Kumar, Y.Y. Fatt, I. Janajreh, Flow-induced vibration and heat transfer in arrays of cylinders: effects of transverse spacing and cylinder diameter, Int. Commun. Heat Mass Transf. 149 (2023) 107159, https://doi.org/10.1016/j.icheatmasstransfer.2023.107159.
[23] A. Bejan, Shape and Structure, from Engineering to Nature, Cambridge University, Cambridge, UK, 2000.
[24] A. Bejan, S. Lorente, Design with Constructal Theory, John Wiley & Sons, Hoboken, N.J, 2008.
[25] A. Bejan, The Physics of Life: The Evolution of Everything, St. Martins Press, New York City, 2016.
[26] Y. Kim, S. Lorente, A. Bejan, Constructal multi-tube configuration for natural and forced convection in cross-flow, Int. J. Heat Mass Transf. 53 (2010) 5121–5128, https://doi.org/10.1016/j.ijheatmasstransfer.2010.07.053.
[27] C. Biserni, F.L. Dalpiaz, T.M. Fagundes, M. Garai, L.A.O. Rocha, Geometric optimization of morphing fins coupled with a semicircular heat generating body: a numerical investigation on the basis of Bejan's theory, Int. Commun. Heat Mass

Transf. 86 (2017) 81–91, https://doi.org/10.1016/j.icheatmasstransfer.2017.05.006.
[28] T. Bello-Ochende, A. Bejan, Constructal multi-scale cylinders with natural convection, Int. J. Heat Mass Transf. 48 (2005) 4300–4306, https://doi.org/10.1016/j.ijheatmasstransfer.2005.05.023.
[29] T. Bello-Ochende, J.P. Meyer, O.I. Ogunronbi, Constructal multiscale cylinders rotating in cross-flow, Int. J. Heat Mass Transf. 54 (2011) 2568–2577, https://doi.org/10.1016/j.ijheatmasstransfer.2011.02.004.
[30] G.M. Barros, G. Lorenzini, L.A. Isoldi, L.A.O. Rocha, E.D. dos Santos, Influence of mixed convection laminar flows on the geometrical evaluation of a triangular arrangement of circular cylinders, Int. J. Heat Mass Transf. 114 (2017) 1188–1200, https://doi.org/10.1016/j.ijheatmasstransfer.2017.07.010.
[31] F.B. Teixeira, C. Biserni, P.V. Conde, L.A.O. Rocha, L.A. Isoldi, E.D. dos Santos, Geometrical investigation of bluff bodies array subjected to forced convective flows for different aspect ratios of frontal body, Int. J. Therm. Sci. 161 (2021) 106724, https://doi.org/10.1016/j.ijthermalsci.2020.106724.
[32] F.B. Teixeira, G. Lorenzini, L.A. Isoldi, E.D. dos Santos, L.A.O. Rocha, Geometric evaluation of bluff bodies arrangement under turbulent flows with mixed convection heat transfer, J. Eng. Thermophys. 32 (2023) 279–311, https://doi.org/10.1134/S1810232823020078.
[33] V.A. Pedroti, C.C. de Escobar, E.D. dos Santos, J.A. Souza, Thermal analysis of turbular arrangements submitted to external flow using constructal theory, Int. Commun. Heat Mass Transf. 111 (2020) 104458, https://doi.org/10.1016/j.icheatmasstransfer.2019.104458.
[34] E.H.T. Cunegatto, M. Gotardo, F.S.F. Zinani, Numerical analysis of tube arrangements with one, two, and four degrees of freedom for heat transfer with pseudoplastic fluids, Int. J. Heat Mass Transf. 208 (2023) 124080, https://doi.org/10.1016/j.ijheatmasstransfer.2023.124080.
[35] A. Bejan, Convection Heat Transfer, fourth ed., Wiley, Hoboken, New Jersey, 2013.
[36] H.K. Versteeg, W. Malalasekera, An Introduction to Computational Fluid Dynamics: The Finite Volume Method, Pearson, 2007.
[37] S.V. Patankar, Numerical Heat Transfer and Fluid Flow, McGraw-Hill, New York, 1980.
[38] Ansys, FLUENT User's Guide, Version 14.0, ANSYS Inc., Canonsburg, PA, USA, 2011.
[39] C. Geuzaine, J.-F. Remacle, Gmsh: a 3-D finite element mesh generator with built in pre- and post-processing facilities, Int. J. Numer. Methods Eng. 79 (11) (2009) 1309–1331, https://doi.org/10.1002/nme.2579.
[40] Y.A. Çengel, J.M. Cimbala, Fluid Mechanics: Fundamentals and Applications, Third edition, McGraw-Hill, 2012.
[41] F. Hilpert, Studien zur Systematik der Trichostomaceen, Beih. Zum Bot. Cent. 50 (1933) 585–706.
[42] E.D. Grimison, Correlation and utilization of new data on flow resistance and heat transfer for cross flow of gases over tube banks, Trans. ASME 59 (1937) 583–594.
[43] K. Momose, H. Kimoto, Forced convection heat transfer from a heated circular cylinder with arbitrary surface temperature distributions, Heat Transf.-Asian Res. 28 (1999) 484–499, https://doi.org/10.1002/(SICI)1523-1496(1999)28:6<484::AID-HTJ6>3.0.CO;2-T.
[44] R.P. Bharti, R.P. Chhabra, V. Eswaran, A numerical study of the steady forced convection heat transfer from an unconfined circular cylinder, Heat Mass Transf. 43 (2007) 639–648, https://doi.org/10.1007/s00231-006-0155-1.